

HYPERFINE STUDIES OF LITHIUM VAPOR USING
SATURATED ABSORPTION SPECTROSCOPY

by
ADRA VICTORIA CARR

Submitted to the Honors College
in partial fulfillment of the requirements for the degree of

Bachelor of Science
with Honors in
PHYSICS
at the
UNIVERSITY OF ARIZONA
MAY 2007

Approved By

Dr. Alexander Cronin
Dept of Physics

STATEMENT BY AUTHOR

This thesis has been submitted in partial fulfillment of requirements for a degree at The University of Arizona and is deposited in the University Library to be made available to borrowers under rules of the Library.

Signed: _____

Contents

1	Introduction	4
2	Setup	5
2.1	Laser Construction	5
2.2	Heat Pipe Oven	7
2.3	Optical layout	8
3	Theory	10
3.1	Fine and Hyperfine Structure of Lithium	10
3.1.1	Fine Structure	10
3.1.2	Hyperfine Structure	11
3.1.3	Lithium Spectrum	12
3.2	Line Shapes	12
3.2.1	how does laser light behave as it goes through the oven?	13
3.2.2	how are electrons excited by the incident light?	13
3.2.3	how do these relations translate into the detected spectra?	14
3.3	Broadening Mechanisms	15
3.4	Saturated Absorption Spectroscopy	16
3.4.1	Cross-over features	18
3.5	Lineshape for Saturated Absorption Spectroscopy	20
4	Observations of Hyperfine Structure	22
4.1	Isotope and D_1 & D_2 Comparison	22
4.2	Buffer gas pressure	23
4.3	Temperature Dependence	25
5	Conclusion	28
6	Appendix	30
6.1	Laser System Control Circuits	30
6.1.1	Temperature Control Circuit	30

Chapter 1

Introduction

Diode lasers have numerous applications ranging from optical data storage and everyday bar-code scanners to advanced spectroscopy systems [4]. With slight modifications, these diodes provide narrow bandwidth light that can be tuned in frequency. Thus they are useful for studying atomic and molecular transitions and demonstrating key concepts in laser spectroscopy and Atomic/Molecular/Optical (AMO) physics.

In this work, I built an extended cavity diode laser (ECDL) along with a saturated absorption spectroscopy system to study the hyperfine structure of the $2S_{1/2} - 2P_{1/2}$ (D_1 line) and $2S_{1/2} - 2P_{3/2}$ (D_2 line) transitions in ^6Li and ^7Li Lithium isotopes. My goal was to observe the atomic hyperfine structure and to understand the spectral line shapes of the Doppler-free saturated absorption features. Using a Lithium heat pipe oven, I performed experiments with different temperatures and buffer gas pressures to see how these variations would affect the spectral line features. I present this data and a theoretical model of the spectral features in this thesis.

Features such as the ones obtained are useful, in principal, for laser stabilization by locking the frequency of a laser with respect to an atomic spectral feature.[20] As such, saturated absorption experiments have applications to experiments requiring a high degree of precision in output laser wavelength, such as BEC and laser cooling and trapping experiments [14]. Another application, in principle, is the ability to map out more complicated molecular spectra with hyperfine structures and isotope shifts that may be difficult to model theoretically with high precision [18]. From the spectra, properties of the atomic vapor samples can also be determined such as number density, concentration, temperature, and hyperfine splitting. [6, 16, 17, 11]

Chapter 2

Setup

The general setup consisted of a single laser whose output was split up into three beams: a pump beam and two probe beams. Shown in Fig 2.1, these probes were generated using the reflections from a peice of 0.5 cm thick glass. The probe beams were only a small fraction of the incident pump beam intensity. Both probe beams were utilized in the experiment, one interacting with normal lithium atoms in the oven, and the other crossing the pump beam and interacting with a group of atoms that had been “pumped” into excited states by the bright beam. The two resultant probe beams were detected with two photodiodes, allowing a difference signal to be created electronically using the circuit shown in Fig 6.5.

2.1 Laser Construction

An extended cavity diode laser (ECDL) was constructed to provide the incident 670 nm light needed to study the D_1 and D_2 transitions in Lithium. The ThorLabs DL3149-057 diode laser and collimating lens were mounted inside an aluminum housing, shown in Fig. 2.2. This aluminum block was heated using two transitors and a resistor, thereby controlling the output wavelength of the laser. The laser’s wavelength was seen to turn redder as its temperature increased. While dependent on the particular diode being used, usual operating temperatures were in the range from 35 – 45°C. The normal operating range for the diode current was in the range of 35-45 mA. This range resulted in an output power of around 2.6mW and a variable range in wavelength of little more than one nanometer. This output power was sufficient to have the intensity of the pump beam be much greater than the saturation intensity of the Lithium atoms. This saturation is discussed more in detail in Chapter 3. The laser itself was controlled with a function generator, supplying a variable amount of current to the laser. Ramping up and down in current with a triangle wave function, the output laser wavelength could also be controlled through a mode-hop free range of about

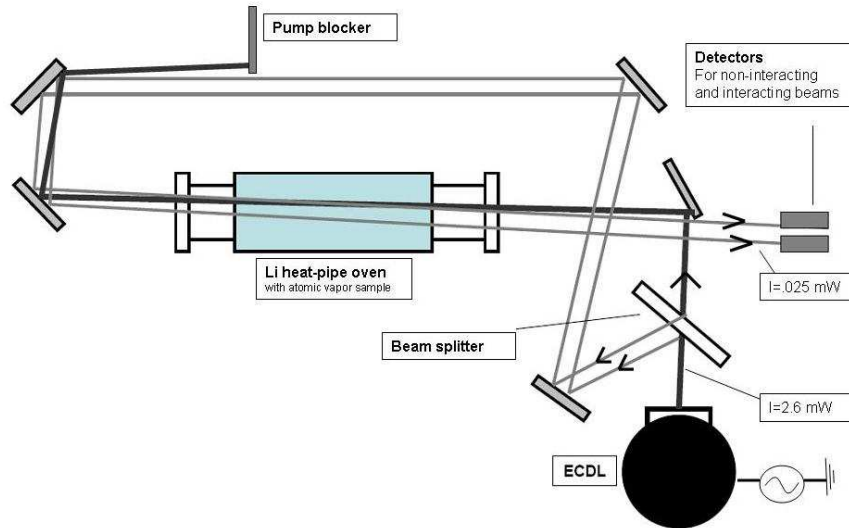


Figure 2.1: Overview of setup with pump and two probe beams. These two beams allow for a difference signal to be observed

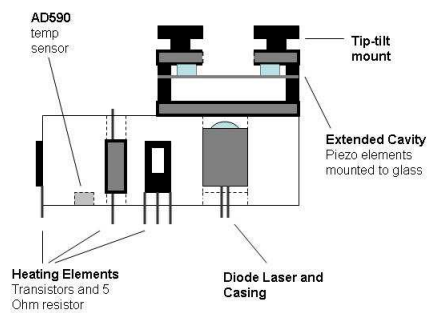


Figure 2.2: Overview of aluminum laser mount. Temperature was stabilized using a AD590 sensor and a home-made feedback controller. The extended cavity served to force the laser to operate in a single mode.

30 GHz. This wide “scanning range” lets us observe the D_1 and D_2 lines of ${}^6\text{Li}$ and ${}^7\text{Li}$ in one single trace. This is seen in Fig 3.1, where all three features are seen on one continuous mode-hop free scan in laser current.

Without the external cavity mirror, the laser, by itself, was seen to be “multi-mode” and seen to have mode hops every 1 GHz. In simplified terms, the laser can be thought of as a cavity in which standing waves are setup as photons propagate through the lasing material. This is responsible for the output wavelength of the laser. However, while one primary wavelength (“mode”) is output, other wavelengths can be fit into the cavity, setting up their own standing waves. While these modes may be weaker, they result in the laser “wanting” to operate in different modes (outputting slightly different wavelengths) as the current is scanned. These small changes in operating wavelength, or *mode hops*, make the resonance features difficult to study. One way to fix this problem is to impose more boundary conditions for our desired standing wave to satisfy. I did this by placing a piece of glass in front of the diode and having the reflection off the front plate feed back into the laser cavity. This effectively forces the laser to operate in one mode with primarily one wavelength that satisfies conditions on both cavities we have created (ie. *single-mode* operation). This piece of glass (in our setup, an uncoated microscope cover slip) is what makes the “external cavity” in our ECDL. It is driven by piezo elements at the same time as the function generator sweeps the laser current in order to compensate for the changes in laser wavelength that occur with varying the supplied current.

A more detailed analysis of the circuits involved in temperature control, piezo control, and laser circuitry can be found in the Appendix.

2.2 Heat Pipe Oven

Experiments with other alkali metals, such as Cesium, may be more easily performed due to the fact that they have a relatively higher vapor pressure at room temperature. However, due to Lithium’s low vapor pressure, it needs to be heated to around $350 - 400^\circ\text{C}$ to obtain a good number density to produce absorption [12]. A heat pipe oven was constructed to accomplish this. Consisting of a stainless steel pipe measuring roughly 16 in. long and 1 1/2 in. in diameter. High vacuum windows were attached at either end to allow the laser to pass through the chamber. A heating coil was wound around the tube and wrapped in insulation. Heat spreaders were placed at either end of the heating coil to try to prevent Lithium from reaching and condensing on the windows. As such, Lithium was seen to eventually build up around this region, reducing the total number density in the chamber, and forcing the Lithium to be replaced after roughly 6 months of use.

Lithium was placed in the middle of the oven while using a Argon gas as a buffer to help prevent oxidation of the pellets. After sealing the chamber,

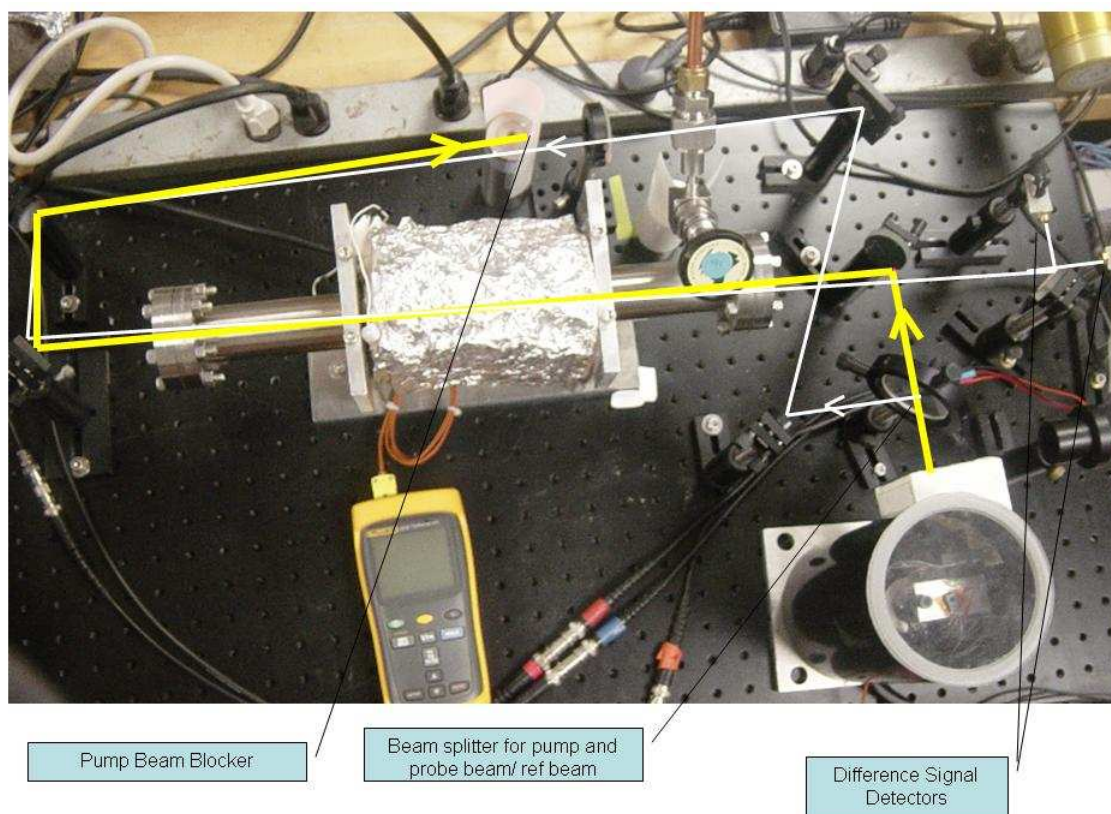


Figure 2.3: physical setup with the beam lines drawn out. The white beam represents the two probe beams (one interacting with the pump beam and one non-interacting).

it was pumped down in pressure while the oven was heated to 300°C . While part of our studies required varying the Argon buffer gas pressure, most hyperfine studies were carried out using roughly 10 mTorr Argon pressure. The oven was then baked out at 500°C to break any oxidation that may have formed on the Lithium. Studies could then be carried out around $350 - 400^{\circ}\text{C}$.

2.3 Optical layout

A 0.5 cm thick piece of glass functioned as a beamsplitter for the two probe beams. While being diverted around the oven, the two probes went through a lens to focus the beams. This provided a more easily detectable beam (due to a small detection area on our detector chips) and ensured that the pump beam was interacting with all parts of the probe. It was found that, when the

probe beam was too large in size, the pump beam would only interact with a small portion of it and the saturated absorption signal would be drowned out by the non-saturated signal resultant from the rest of the beam.

The pump beam was sent through the oven and then propagated partially back through the system. This unwanted back-reflection was blocked by a card to ensure that it would not cause feedback into the laser cavity.

Chapter 3

Theory

3.1 Fine and Hyperfine Structure of Lithium

Before discussing the structure of Lithium in particular, it is helpful to first review how the fine and hyperfine structures arise. Specifically, the allowed transitions will be discussed, leaving a more detailed discussion of energy levels modifications to Ref [2, 7, 3].

3.1.1 Fine Structure

Fine Structure splitting of energy levels arise due to adding magnetic interactions into our model of the atom. We model a electron as orbiting its nucleus with angular momentum, \mathbf{L} . Due to the charge of the electron, this orbital motion gives rise to a magnetic dipole moment, μ . In quantum theory, the electron also has a magnetic moment due to its spin, $\mu_S = \mu_B \mathbf{S}$. These two magnetic moments can interact depending on the orientation of the spin, \mathbf{S} , and orbital angular momentum, \mathbf{L} , vectors.

The total angular momentum of the electron is expressed in terms of a new quantum number, \hat{J} , where

$$\hat{J} = \hat{L} + \hat{S} \quad (3.1)$$

The allowed values it can take can be derived from the rules of addition of angular momentum.

$$\hat{J}^2 : \hbar^2 J(J + 1) \quad |L - S| \leq J \leq L + S \quad (3.2)$$

$$\hat{J}_z : \hbar m_J \quad -J \leq m_J \leq J \quad (3.3)$$

For the S-state ($L=0$), J can only be $1/2$. For the P-state($L=1$), J can be $1/2$ or $3/2$. This gives rise to the $2P_{1/2}$ and $2P_{3/2}$ states which are separated in energy by 10^{-4} eV for Lithium atoms. The spectral signal of the fine structure splitting in Lithium is two absorption lines separated by 10 GHz (.015 nm). The doppler broadened fine structure of Lithium demonstrating

J value splitting can be seen in Fig. 3.1. The D_1 line is the $S_{1/2}$ to $P_{1/2}$ transition and the D_2 line is the $S_{1/2}$ to $P_{3/2}$ transition. The doppler width, discussed in Section 3.3, is 3 GHz and the isotope shift is 10GHz. This means that the two isotope absorption features of ${}^6\text{Li}D_2$ and ${}^7\text{Li}D_1$ overlap in our resultant spectra.

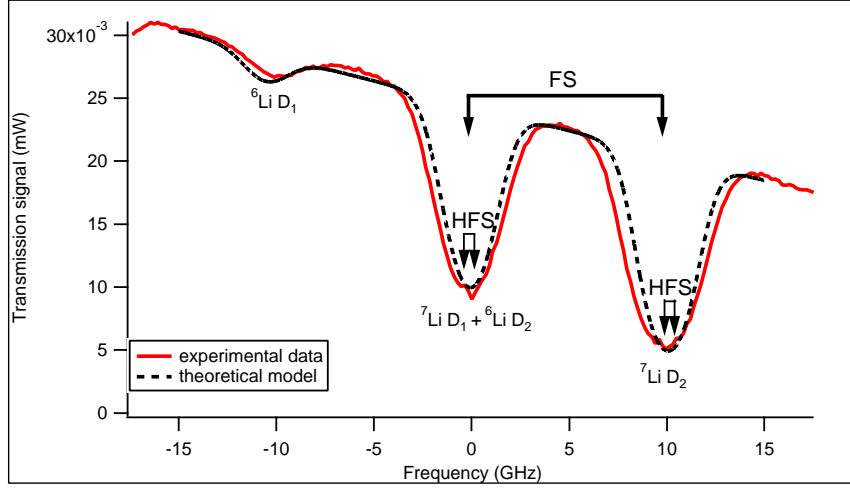


Figure 3.1: Absorption spectrum of ${}^6\text{Li}$ and ${}^7\text{Li}$. The 3 large absorption features are explained by fine structure and isotope shifts. The known fine structure splitting was used to establish the frequency axis. Saturated absorption features due to hyperfine structure are present at the base of the fine structure features, but these are very small. Difference between theoretical model and data could be due to other broadening mechanisms not accounted for (like saturation and collisional broadening).

3.1.2 Hyperfine Structure

The fine structure took into account the interaction between the magnetic moment of the current due to the electron's orbit and the intrinsic magnetic moment of the electron due to its spin. It also took into account relativistic effects on energy levels. The next effect that must be considered is the interaction between the total magnetic moment of the electrons, J , with the nuclear magnetic moment due to nuclear spin, I . Again, we can then define a new quantum number \mathbf{F} , such that

$$\hat{F} = \hat{J} + \hat{I} = \hat{L} + \hat{S} + \hat{I} \quad (3.4)$$

Due to the angular momentum addition rules governing J and I angular momenta, we can determine F and m_F states as

$$\hat{F}^2 : \hbar^2 F(F + 1) \quad |I - J| \leq F \leq I + J \quad (3.5)$$

$$\hat{F}_z : \hbar m_F \quad -F \leq m_F \leq F \quad (3.6)$$

This leads to the hyperfine structure splitting, whose energy can be modeled by

$$\Delta E_F \propto \hat{J} \cdot \hat{I} \quad (3.7)$$

3.1.3 Lithium Spectrum

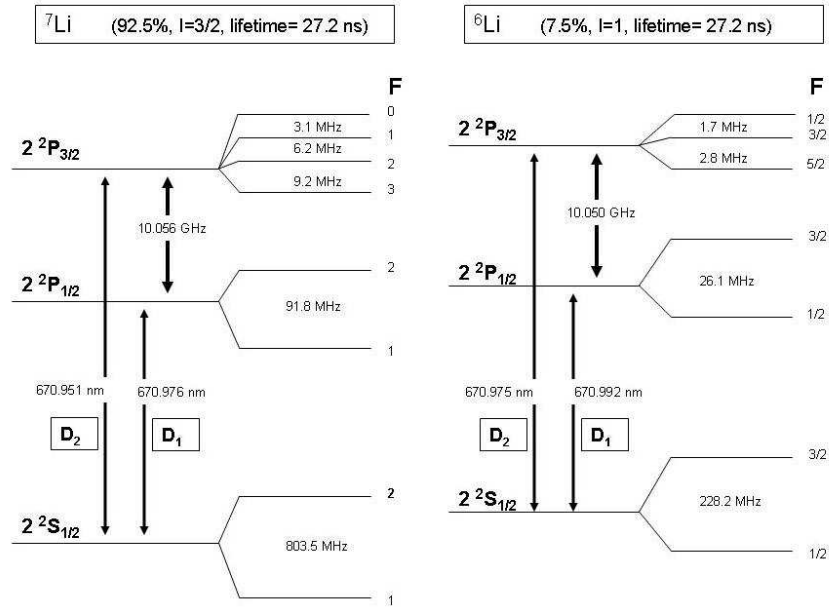


Figure 3.2: Energy level diagram for the S and P levels in ${}^6\text{Li}$ and ${}^7\text{Li}$ isotopes. Due to the small isotope shift in energy levels, each spectrum can be observed within a small frequency range. [12]

An energy level diagram for the lithium fine and hyperfine structure is shown in Figure 3.2. Lithium is an alkali atom, hence it has only one valence electron outside a closed shell. This “hydrogen-like” property allows for a relatively uncomplicated energy level system to probe. It should be noted that the most abundant isotope of Lithium is ${}^7\text{Li}$, with only a small natural abundance of ${}^6\text{Li}$ (92.5 to 7.5% respectively). Therefore, our ${}^7\text{Li}$ features are deeper and more dominant in the observed spectra.

3.2 Line Shapes

In order to quantitatively understand the spectra that we observe, we can ask ourselves a series of questions to help understand the quantities being derived. These quantities will be central in generating the theoretical model

used to compare our resultant data to.

- 1) how does laser light behave as it goes through the oven?
- 2) how are atoms excited by the incident light?
- 3) how do these relations translate into the detected spectra?

These questions will be handled one-by-one to “walk through” the process of deriving the lineshapes of our absorption features. A more thorough derivation of these quantities can be found in [10, 7].

3.2.1 how does laser light behave as it goes through the oven?

If one was to shine the laser light through the oven, how much power would be transmitted through the vapor? Answering this will allow us to have some idea of a “baseline” in which to model our absorption features with. The transmitted power of the laser light is related to the initial power of the light by the coefficient of absorption, $\alpha(\omega)$. Specifically

$$\frac{1}{P_t(x)} \frac{dP_t(x)}{dx} = -\alpha(\omega) \quad (3.8)$$

where x is the longitudinal position in the vapor. Solving for transmitted power gives

$$P_t(x) = P_0 e^{-\alpha(\omega)x} \quad (3.9)$$

This will be the function that is plotted in our theoretical model since it is essentially just the power reaching our detector. To define the absorption coefficient, the light’s interaction with the atoms themselves needs to be analyzed.

3.2.2 how are electrons excited by the incident light?

The initial population of the ground state is taken to be n_1 . Assuming that there is little to no excitation to the excited states in the atom, we can assume the excited state initial population to be zero ($n_2 = 0$). The populations of the states addressed by the laser (ie the ground state population) can then be related to $\alpha(\omega)$ through an absorption cross section, $\sigma(\omega)$

$$\alpha(\omega) = n_1 \sigma(\omega) \quad (3.10)$$

So this tells how the population of the atomic states affects the incident light.

3.2.3 how do these relations translate into the detected spectra?

To simplify things, all frequency dependencies that we have been using can be summed up in one line shape function term, $g(\omega)$. Normalizing appropriately over all frequencies, this means that the old quantities of $\alpha(\omega)$ and $\sigma(\omega)$ can be expressed in terms of $g(\omega)$.

$$\alpha(\omega) = \alpha_0 g(\omega) \quad (3.11)$$

$$\sigma(\omega) = \sigma_0 g(\omega) \quad (3.12)$$

where $\alpha(\omega)$ and $\sigma(\omega)$ are the frequency integrated absorption coefficient and cross section [10].

So, relating $\alpha(\omega)$ to σ_0 , we need to be able to express σ_0 in terms of known quantities. This can be done by using Einstein coefficients saying that

$$\sigma_0 = \frac{1}{4} \left(\frac{g_2}{g_1} \right) \lambda_{21}^2 g(\omega) A_{21} \quad (3.13)$$

where state 2 is the excited state and state 1 is the ground state. The g factors correspond to the degeneracies of each respective state. Having a full expression for the coefficient of absorption, we can now analyze our lineshape function, $g(\omega)$.

At first glance, it might be assumed that the lineshape function for the absorption spectra would be a series of infinitely sharp delta functions corresponding to the frequencies at which absorption occurs. This is because, given the finite energies of each of the energy levels, a definitive wavelength of light can be calculated that would cause an electron in the ground state to be excited, namely

$$\omega_{12} = \frac{(E_2 - E_1)}{\hbar} \quad (3.14)$$

However, every excited state decays with a certain lifetime, τ . Due to the uncertainty principle, this means that each energy state must have an associated uncertainty of order $\frac{\hbar}{\tau}$. This leads to a natural width of an energy level. Relating this to the final absorption spectrum, we have a *natural linewidth* that is modeled by a Lorentzian function

$$g_L(\omega) = \frac{(\gamma_{ik}/2)^2}{(\omega - \omega_{ik})^2 + (\gamma_{ik}/2)^2} \quad (3.15)$$

where γ_{ik} is the natural linewidth and ω_{ik} is the angular frequency of the transition from states i to k [2]. For our case, our γ_{ik} is 5.96MHz [15]. To simplify notation, we can write ω_{ik} just as ω and take the transition as always being from the ground state. ω_0 is then defined as the resonant frequency of the transition. With this expression for linewidth, we can build

a full expression for the absorption coefficient

$$\alpha(\omega)_{ik} = n_i(\sigma_0)_{ik} \frac{(\gamma_{ik}/2)^2}{(\omega - \omega_{ik})^2 + (\gamma_{ik}/2)^2} \quad (3.16)$$

This allows us to generate the absorption coefficient for each of the transitions in our hyperfine structure. Now we need to see how this lineshape changes when we factor in the behavior of the atoms in our vapor cell.

3.3 Broadening Mechanisms

If every feature were able to be resolved to its natural linewidth, hyperfine studies would be much easier to perform. However, the Lorentzian lineshape derived previously did not take into account one important factor of our system: the elements we are trying to study are moving. Calculating the v_{rms} of the atoms using the relation that $\frac{1}{2}mv^2 = \frac{3}{2}k_bT$ and $(v_x)_{rms} = \frac{1}{\sqrt{3}}v$, we find that for an oven temperature of 350°C our atoms are moving around 850m/s . This means that, along the direction of the laser (which is all we are concerned with), there is a large non-zero velocity component of our studied atoms at any given time. This introduces *Doppler broadening* into our spectral lineshape. Considering an atom traveling “with” the direction of the incident beam, it will see the wavelength of laser light as redshifted, consequently being resonant at a higher frequency, bluer wavelength than expected (with the opposite being the case with a atom traveling “against” the incident beam). This will result in a larger frequency range that will produce absorption. Specifically, this lineshape can be modeled as a gaussian

$$g_D(\omega) = e^{-\frac{c^*(\omega-\omega_0)^2}{\omega_0^2*v_p}} \quad (3.17)$$

where $v_p = \sqrt{\frac{2k_bT}{m}}$. To produce the correct lineshape taking this effect into account, these lineshape functions must be convolved with one another. This results in a Voigt profile lineshape. With this new $g_v(\omega)$ calculated, a new $\alpha(\omega)$ can be found using Eq 3.11 and its value plugged into our original expression for $P_t(x)$. This can be done after normalizing the Doppler lineshape to 1. This adds an additional normalization constant of $\frac{c}{\sqrt{\pi}\omega_0 v_p}$ to our g_D function. This new profile has a FWHM according to

$$\Delta\omega_D = \frac{2v_p\omega_0}{2}\sqrt{\ln 2} \quad (3.18)$$

This is about 1.5 GHz for our distribution[7].

Other broadening mechanisms can also contribute to this larger frequency range of absorption. Understanding of broadening due to pressure, collisions with other atoms, incident beam intensity, etc are essential in determining what *next* limits our resolution once the doppler broadening of

our features is eliminated. A table of relative spectral widths is shown to have an idea of how each broadening mechanism and energy perturbation affects the resultant spectra.

Spectral Dependence	$\Delta\lambda$ (nm)	$\Delta\nu$	Δcm^{-1}
$^7\text{Li } D_1$ Feature wavelength	670.976	$4.47 * 10^5$ GHz	14903.67
Grating Spectrometer	.5	330 GHz	11.1
Fine Structure	1.5×10^{-2}	10GHz	.33
Doppler Width	4.5×10^{-3}	3GHz	.01
Hyperfine Structure	1.2×10^{-3}	803MHz	.026
Smallest observed feature seperation	7.5×10^{-5}	50MHz	.0017
Power Broadening	7.5×10^{-5}	50MHz	.0017
Residual Doppler Broadening	4.5×10^{-5}	30MHz	.0001
Saturated Abs signal widths	3.0×10^{-5}	20MHz	.0007
Natural Lifetime	9×10^{-6}	6 MHz	.0002
Transit Broadening (1mm beam)	1.5×10^{-6}	1 MHz	.00003
Pressure Broadening (100mTorr Ar)	1.5×10^{-6}	1MHz	.00003

Table 3.1: Relative spectral widths of spectral features and broadening mechanisms. Hyperfine structure seperation is the largest seperation in ^7Li . Smaller hyperfine seperation can be found in Fig 3.2. Residual doppler broadening is estimated for an angle between atomic trajectory and beam of 10^{-2} rad.

3.4 Saturated Absorption Spectroscopy

In order to regain resolution of the hyperfine spectrum lost due to Doppler broadening, a monochromatic laser can be scanned in frequency by varying the current supplied to it. The laser beam is then split into two beams, an intense “pump beam” which excites a considerable portion of the atoms in the vapor to an excited state and weaker “probe beam” which will resolve the hyperfine spectrum. To first get an idea of how this resolution is obtained, only one resonance feature will be discussed first, followed by the more complicated discussion of several hyperfine features. If only one of the beams were incident on the vapor cell, the usual absorption spectrum would be produced. Instead, the pump beam is sent through the vapor cell “backwards” while the probe is sent through the cell to a detector. Since the frequency of the laser is being scanned through some amount $d\nu$, the atoms in the vapor see two unique doppler-shifted frequencies. This is shown in Fig. 3.3.

Considering an atom with a velocity going “with” that of the probe beam, it will be on resonance with a specific transition at a frequency higher than ν_0 since the probe beam light will be redshifted. Specifically, the atoms

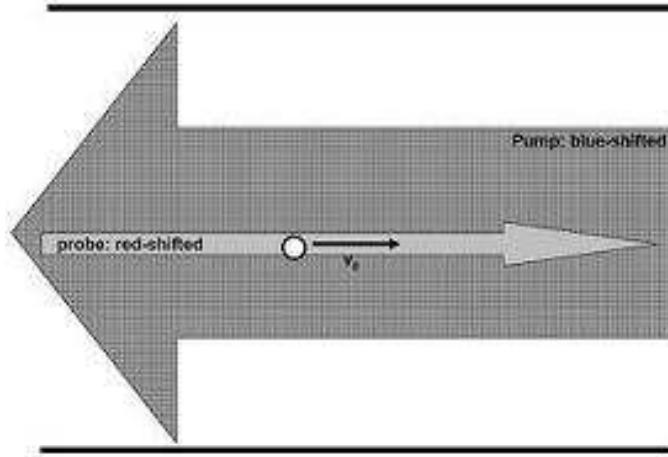


Figure 3.3: Description of atomic interaction with counter-propagating beams in Lithium oven.

would absorb photons with frequency

$$\nu = \nu_0(1 + v/c) \quad (3.19)$$

However, the pump beam will be seen as blueshifted, making the resonant transition frequency lower than ν_0 . Thus, at any given time in the cell, the two beams excite two unique velocity classes, one with $+v$ and one with $-v$. This is seen in Fig. 3.5. Due to the two ground states of our system, $F=1$ and $F=2$, the population from state 1 is excited and decays to state 2. Similarly, the state 2 population is pumped to state 1. We can therefore model this excitation of the two separate velocity classes by looking at the populations of the two ground states. This dip in the population of the ground state and increase in population in the excited state (and therefore the 2nd ground state) is called a *Bennett hole/ dip*. This is shown in Fig 3.4. It should be noted that these two velocity classes still produce the same doppler shifted resultant spectrum. However, when the frequency of the laser is scanned and both the probe and the pump beam are on resonance with the *stationary* velocity class at the transition frequency ν_0 , this doppler broadening is eliminated. Since the pump beam has the effect of exciting a portion of the atoms on resonance, the probe beam excites only a small number of stationary atoms with no resulting doppler shift. This is seen in the spectrum in the form of a decreased absorption peak (*suppressed absorption*), with a very narrow profile compared to that of the Doppler profile. This allows us to resolve smaller features, like that of the F structure, that normally would have been washed out by the doppler broadening of the absorption features.

The width of the doppler-free feature is now limited by other factors in

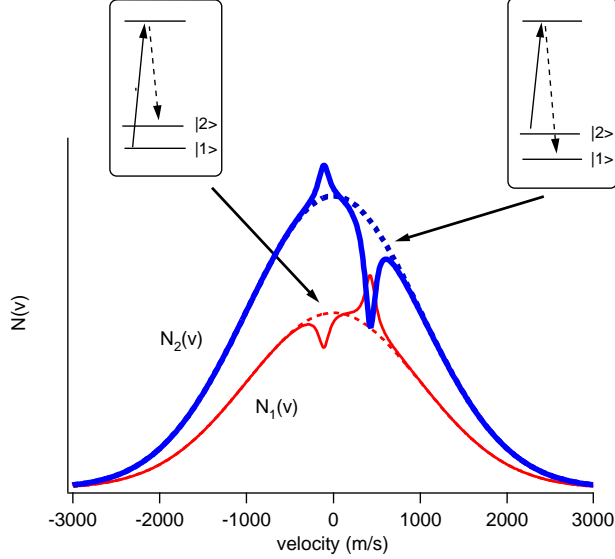


Figure 3.4: Populations of two ground states demonstrating pumping from one state to the other due to an incident laser beam.

the system like power, pressure, and collisional broadening. [5] The quantitative discussion of this new lineshape is discussed in the following section.

3.4.1 Cross-over features

This situation becomes a little more complicated when more than one transition is in the range of the scanning frequency (ie the closely spaced hyperfine spectrum). In the case of two features in the scanning range, ν_1 and ν_2 , a feature also arises when the laser frequency is halfway between the features. This can be derived by taking into account the doppler shifts in the resonant frequencies. Considering a group of atoms in a certain velocity class, v_α , the shift in resonant frequency will be ν_α . This means that the excitation by the *pump* beam that will produce the ν_1 feature will be

$$\nu_1 = \nu_L + \nu_\alpha \quad (3.20)$$

where ν_L is the operating laser frequency. The *probe* beam will be resonant at, for the same velocity class of atoms

$$\nu_L - \nu_\alpha \quad (3.21)$$

If this frequency corresponds to the other transition, ν_2 , than there will again be absorption and saturation by the atoms. So writing that

$$\nu_2 = \nu_L - \nu_\alpha \quad (3.22)$$

We then can solve for the laser frequency where these conditions are met at [13]. This gives

$$\nu_L = \frac{(\nu_1 + \nu_2)}{2} \quad (3.23)$$

Therefore, at a frequency half-way between the two transitions, the probed atoms are again depleted from the resonant state. This is shown as the intersections of state 1 with state 2 in Fig. 3.5. The resonance can either cause a decrease in the population density of a common lower level or an increase in population of a common upper level. This can produce a feature with either increased or decreased absorption. [5].

Considering a case with two excited states and one ground state (like in Cesium) referred to as a \mathbf{V} configuration, the pump and probe beams both excite atoms out of the ground state and into the excited states, then quickly decaying to other hyperfine states 9 GHz away. This results in a suppressed absorption feature due to the lowered number of atoms available in the ground state for excitation. In our case, we consider a Λ configuration was

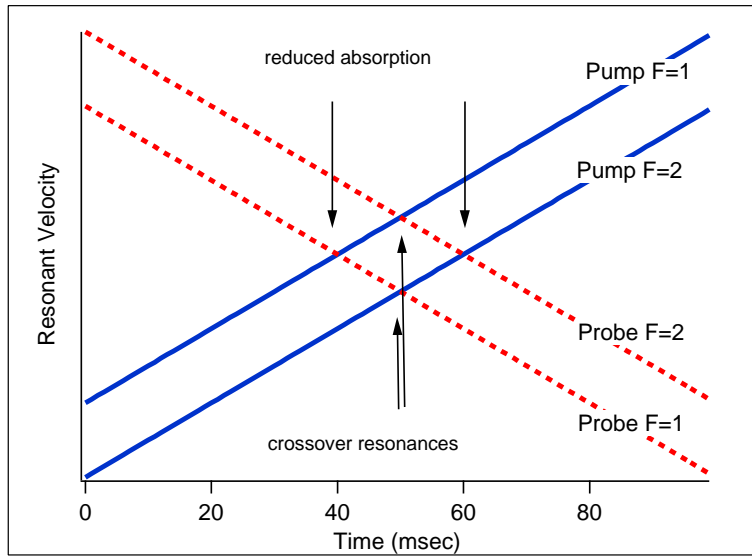


Figure 3.5: Scan of pump and probe beams' resonant velocity classes over time. Intersections of same states result in resonances with stationary atoms and hence the produced suppressed absorption feature. Intersections of state 1 with state 2 show conditions for crossover resonance features.

two ground states and one excited state. In this configuration, both beams are pumping (via the excited state) atoms into the other ground state. This results in an increased number of atoms to excite, yielding an increased absorption feature like that seen in Fig 3.6.

With this model, we can now sufficiently explain each feature seen in our resolved hyperfine structure.

3.5 Lineshape for Saturated Absorption Spectroscopy

Quantitatively, we can look at our produced doppler-free signal in terms of population differences that arise in the studied atoms. Previously, our absorption coefficient was defined as

$$\alpha(\omega) = n_1\sigma(\omega) \quad (3.24)$$

Instead of absorption due to a certain state in the atom, we can look at the absorption due to a certain group of atoms in a specific velocity class. This leads to a slightly more complicated, yet equivalent expression of

$$\alpha(\omega) = \int N(v)\sigma(\omega - kv)dv \quad (3.25)$$

In this case, we have looked at the absorption coefficient for a certain velocity class of atoms moving in the range v to $v + dv$. $N(v)$ is the number density of atoms in this velocity class and the $\sigma(\omega - kv)$ term would be due to the fact that atoms with velocity v to $v + dv$ would have a effective frequency of $\omega - kv$ in our rest frame [7]. This expression would ultimately lead to the same derivation of the Voigt profile found earlier.

Now for saturated absorption. If the intensity of the incident light is low, then relatively few atoms are put into the excited state. This allows stimulated emission and spontaneous relaxation to be neglected. At high intensities of incident light though, the population difference between the ground state and excited states is appreciably reduced and must be accounted for. This point where excited states are significantly filled can be described as “saturation”. The new expression for our absorption coefficient taking this difference into account can then be expressed as

$$\alpha(\omega) = \sigma_0\Delta N g_L(\omega) \quad (3.26)$$

We can then try to determine the intensity at which this saturation occurs. The saturation parameter can be defined as the ratio of the number of photons involved in induced transitions from the upper to lower state to the number of photons emitted in spontaneous transitions. This is defined as

$$S_0 = \frac{2P}{R_1 + R_2} \quad (3.27)$$

where P is the probability of induced transitions, R_1 is the rate of spontaneous excitation, and R_2 is the rate of spontaneous relaxation [5]. However, we know from our previous discussion that profile absorption coefficient had a frequency dependence that was modeled by a Lorentzian. This means that our the probability of absorption would also have some frequency dependence. This allows us to rewrite the saturation parameter as dependent on ω

$$S_\omega = S_0 \frac{(\gamma/2)^2}{(\omega - \omega_0)^2 + (\gamma/2)^2} \quad (3.28)$$

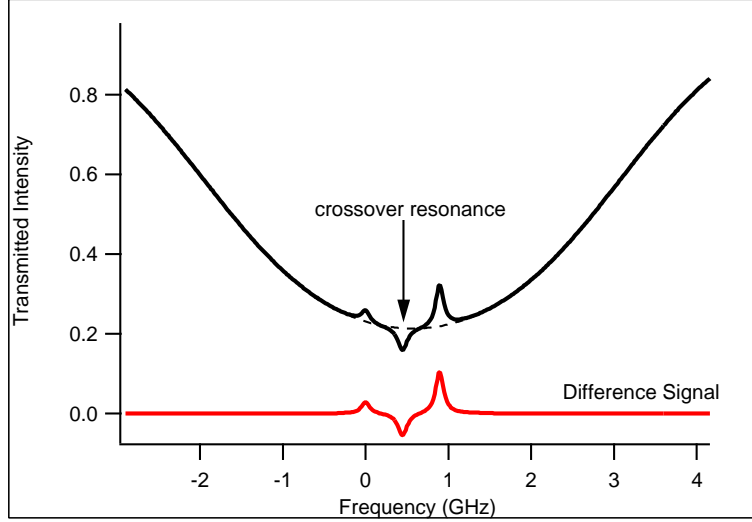


Figure 3.6: Theoretical model of a Λ configuration system. The top function shows the the saturated absorption signal with doppler broadening. The bottom signal shows the difference between saturated absorption and doppler broadened signals.

Taking this population difference into account in the absorption coefficient, we can express this as

$$\alpha_S(\omega) = \frac{\alpha_L(\omega)}{1 + S_\omega} = \alpha_0 \frac{(\gamma/2)^2}{(\omega - \omega_0)^2 + (\gamma_S/2)^2} \quad (3.29)$$

where $\gamma_S = \sqrt{\gamma + S_0}$. With this new expression for our absorption coefficient, we can calculate the intensity for saturation. This $I_{sat} = 2.56 \frac{mW}{cm^2}$ for ${}^7\text{Li}$ [15]. Our pump beam must be on this order to produce a resolved saturated absorption spectrum.

Looking at specifically at the difference in population, we can see that it is directly related to the intensity of the incident light. Specifically, this width (derived similar to that for Doppler broadening width) can be modeled in terms of this saturation intensity just derived

$$\Delta\omega_{hole} = \gamma_{12} \left(1 + \frac{I}{I_{sat}}\right)^{1/2} \quad (3.30)$$

This means that our pump and probe beams will have different $\Delta\omega_{hole}$ due to their differing intensities. This new expression for resultant intensity can be roughly modeled in Fig 3.6, showing the saturated absorption signal for a Λ configuration such as Lithium.

By giving a more quantitative discussion of saturated absorption by modifying previously derived quantities like $\alpha(\omega)$ and $\Delta\omega$, one can begin to have a better grasp of what dictates the spectral lineshapes of our studied spectra.

Chapter 4

Observations of Hyperfine Structure

4.1 Isotope and D_1 & D_2 Comparison

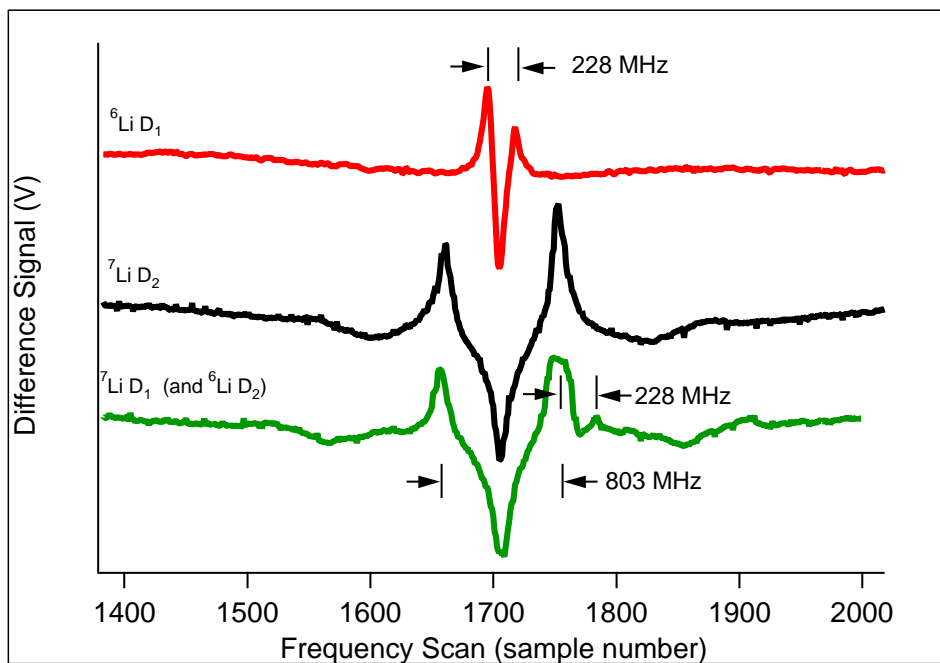


Figure 4.1: Difference signal for the D_1 and D_2 lines for ${}^7\text{Li}$ and ${}^6\text{Li}$. Since all data was collected with the same scanning parameters, scans for each transition can be plotted together to show relative frequency spacing. An offset was added to show features stacked on top of each other for comparison.

While the isotopes of ${}^6\text{Li}$ and ${}^7\text{Li}$ have similar fine structure splitting, the splittings of ${}^6\text{Li}$ hyperfine F levels are much more closely spaced. The ground state splitting for ${}^6\text{Li}$ is 228 MHz, while ${}^7\text{Li}$ has a four times larger splitting with 802.5 MHz. These splittings are consistent in both the D_1 and D_2 lines, with the ${}^6\text{Li}$ splitting still being apparent in the composite D_1/D_2 resonance line.

While the D_1 and D_2 lines of ${}^6\text{Li}$ appear very similar due to their close hyperfine splitting (our system was not able to resolve the finer spaced hyperfine features, especially due to its weaker signal strength) the D_1 and D_2 features of ${}^7\text{Li}$ show some differences. As seen in Fig 3.2, the D_1 line of ${}^7\text{Li}$ has a significant (90 MHz) splitting of its $P_{1/2}$ state between F=1 and F=2. This results in a somewhat more complicated structure, evident as the more flat-bottomed transition in Fig 4.1 that compared to the ${}^7\text{Li}$ D_2 transition. The ${}^7\text{Li}$ D_2 feature can only be resolved with its ground state splitting due to the extremely close spacing of the D_2 excited states. This results in the more sharply peaked features.

4.2 Buffer gas pressure

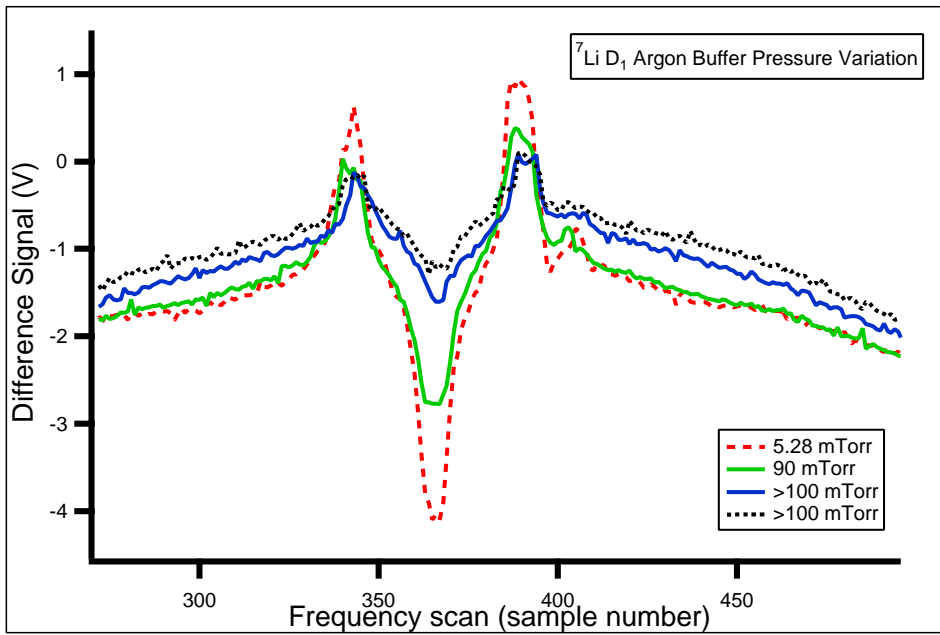


Figure 4.2: Difference signal of hyperfine structure for the blue ${}^7\text{Li}$ D_1 line. Relative offsets of each line have *not* been subtracted to show systematic offset.

The ${}^7\text{Li}$ D_1 feature was observed while the Argon buffer gas pressure was

increased from 5 mTorr to greater than 100 mTorr. The resultant feature is plotted in Fig. 4.2. The depths of the features can be seen to decrease as the buffer gas pressure is increased.

The decrease in depth of the hyperfine features can be understood in the context of time scales of the atom. As the buffer gas pressure is increased, more collisions occur between the Lithium atoms and the Argon buffer atoms. This means that the mean time between collisions in the gas decreases. Calculating this length between collisions, we can use the ideal gas law to derive a number density of the atoms in the vapor.

$$\frac{n}{V} = \frac{P}{k_B T} \quad (4.1)$$

Defining the mean length between collisions (mean free path) as the point where the probability of the atom having not collided drops to $1/e$, we can define a probability of atomic interaction being

$$P = e^{-(N/V)\sigma L} \quad (4.2)$$

From here we can solve for L

$$(1/e) = e^{-(N/V)\sigma L} \quad (4.3)$$

$$L = \frac{-k_B T}{P\sigma} \quad (4.4)$$

Taking the cross section for interaction, σ , as about 1 \AA (the size of an atom), this is roughly 1 mm at low pressure. At higher pressure, this mean free path decreases. These changes in mean free path length directly effect the redistribution time of the atoms in the vapor. At low pressure, the ground state has a certain thermal population. With excitations in the vapor due to the incident laser light, this population is changed. Over time, with the help of collisions from buffer gas atoms, this initial population can be reattained. This redistribution time due to collisional relaxation increases as the pressure in the gas decreases. This means that as the pressure increases, the saturation effects that we have tried so hard to attain in our setup become less significant since the system is able to redistribute itself so quickly. This leads to the decrease in saturated absorption signal with increased pressure seen in Fig. 4.2. Surprisingly, the widths of the features were not seen to drastically change with increase in pressure, suggesting almost negligible effects of collisional broadening in the system.

The crossover resonance can be seen to decrease more drastically than the depths of the actual hyperfine features. This is the best example of the competition between optical pumping to excited states and collisional relaxation. With high buffer gas pressure, the collisional relaxation that goes between the lower states of the atom (ie one velocity group to another) causes an increase in transmission in the vapor [6]. This results in the decreased difference signal.

4.3 Temperature Dependence

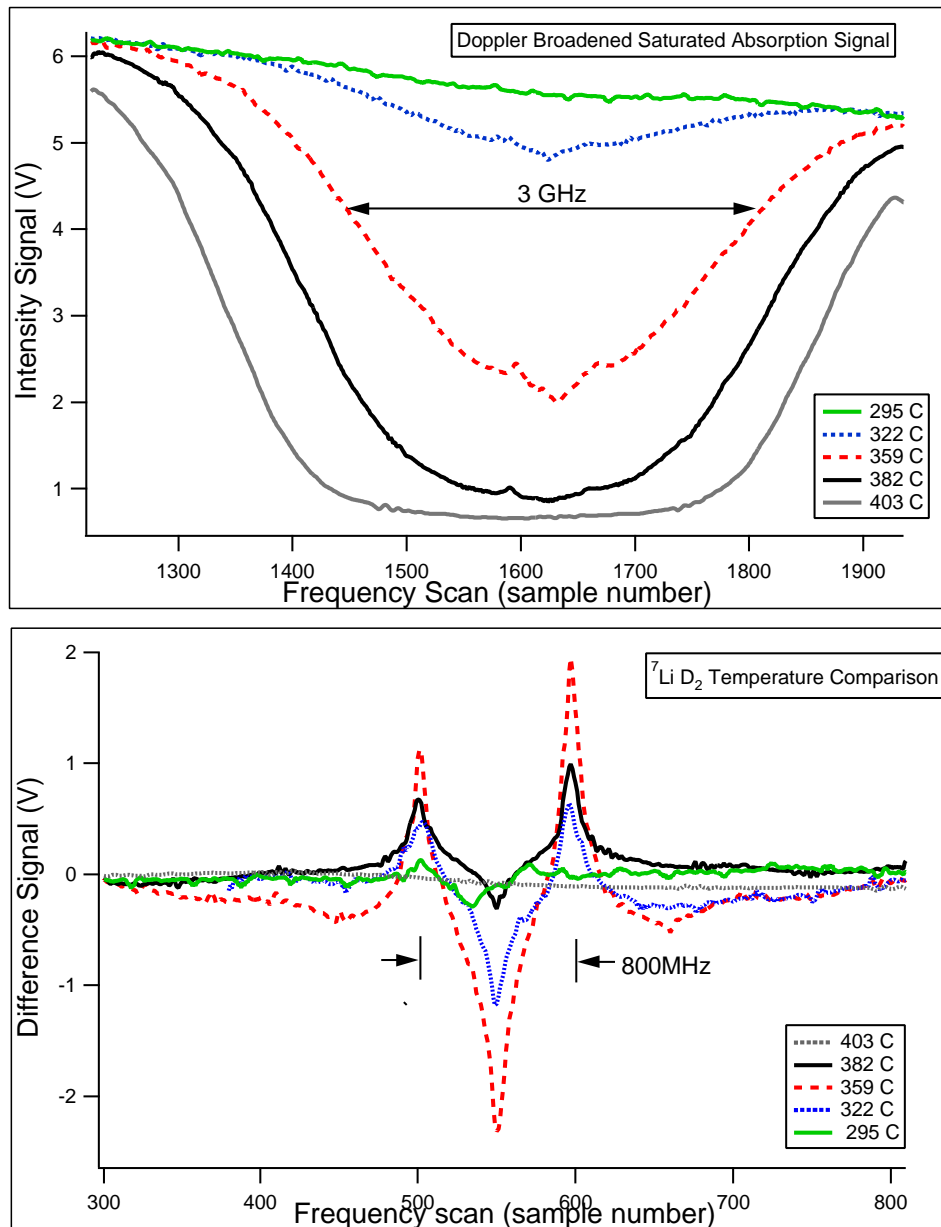


Figure 4.3: Doppler broadened (top) and difference signal (bottom) showing absorption at a series of temperatures for the blue ${}^7\text{Li } D_2$ line. As temperature increased, the doppler broadened signal bottomed out at some offset voltage from zero. This suggests a finite amount of off-mode light originating from the laser.

The difference signal was analysed while changing the temperature of the vapor from 420 °C to 275 °C. At high temperatures, the signal was seen to be weak resultant from little light getting through the vapor due to high number density of the Lithium atoms. At low temperatures, the number density was too low to produce a resolved absorption signal. Between these two extremes, a maximum in signal was seen. This behavior is seen in Fig. 4.3 with four unique values of vapor temperature plotted.

This allows us to ask the question of when is there a max in signal intensity as a function of temperature. We can generalize this question by considering the signal intensity as a function of optical depth, where optical depth is modeled as

$$OD = n\sigma L \quad (4.5)$$

where n is the number density of a given probed portion of atoms in the vapor. We can model the resultant intensity signal of the hyperfine feature as the difference signal from our two probe beams

$$S = I_0 e^{-n_1\sigma L} - I_0 e^{-n_2\sigma L} \quad (4.6)$$

We can relate the two population densities by some factor, f , since the interacting probe beam will be probing a slightly smaller number of atoms in the ground state due to saturation from the pump beam. This allows us to express our exponential in terms of our defined optical depth

$$S = I_0 e^{-OD} - I_0 e^{-OD*f} \quad (4.7)$$

We can differentiate this expression and set it equal to zero in order to find a maximum in signal.

$$OD = -\frac{\ln(f)}{1-f} \quad (4.8)$$

This gives us an expression to predict the optical depth corresponding to a peak value of signal. By looking at this expression, we can see this quantity is only dependent upon the fraction relating the number density of atoms probed by one probe beam versus the other. To verify this graphically, we can plot optical depth versus signal. We can derive a relationship for optical depth by looking at the intensity signal for one beam. Accounting for off mode light, we can model intensity as the fraction of light absorbed versus the starting intensity

$$e^{-OD} = \frac{I_{min} - I_{off}}{I_{max} - I_{off}} \quad (4.9)$$

Solving for optical depth we have

$$OD = -\ln\left(\frac{I_{min} - I_{off}}{I_{max} - I_{off}}\right) \quad (4.10)$$

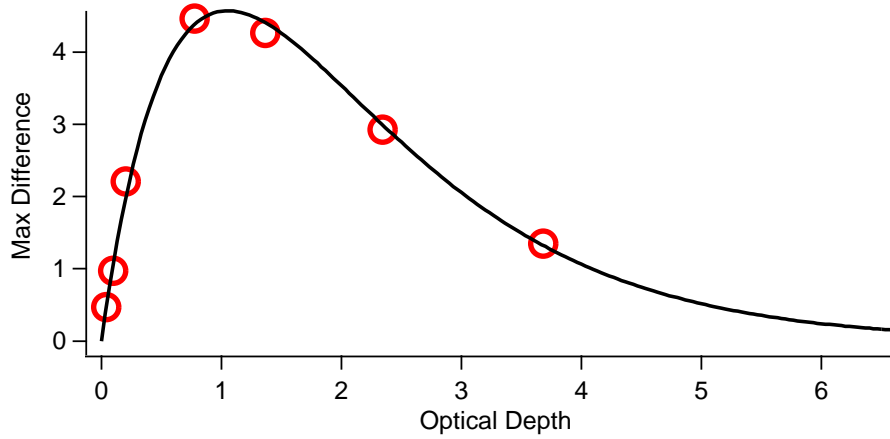


Figure 4.4: Optical depth vs signal plot. The curve shows theoretical model and points show optical depth data taken from varying the temperature of the oven.

This, along with Eq. 4.7 gives us the ability to model optical depth vs signal, shown in Fig. 4.4. This maximum in signal is seen to occur at around 1.1. Using Eq. 4.8 this yeilds a f value of .953. This fit was modeled with one free parameter accounting for the gain of the electronics in our system. Through more measurements of this gain, this free parameter could be eliminated, giving a better model of the actual system.

Chapter 5

Conclusion

Using a home-made laser and a Lithium heat-pipe oven, I created a saturated absorption spectroscopy system and resolved hyperfine transitions in ${}^6\text{Li}$ and ${}^7\text{Li}$. The hyperfine splitting of the ground states in both isotopes could be well resolved. This splitting of 228 MHz in ${}^6\text{Li}$ and 803 MHz in ${}^7\text{Li}$ was well resolved even in the composite ${}^6\text{Li } D_2 / {}^7\text{Li } D_1$ spectral feature, making possible studies of isotope shift. Theoretical models of the hyperfine structures in Lithium with a simplified Λ configuration showed good agreement with experimental data. A more detailed model could be created, taking into account the hyperfine structure of the excited states, but this would produce a model that would only be useful with increased resolution of our system.

Experiments with variation in oven temperature and buffer gas pressure were also performed. Higher buffer gas pressure was seen to produce a reduced saturated absorption signal. However, collisional broadening effects did not significantly influence the width of the resultant features. By varying temperature in the oven, effects of atomic number density could be seen on resultant signal. This variation of optical depth could be modeled and compared to experimental data. This data showed good agreement with a theoretical model.

The limiting factors in our spectral resolution are primarily due to residual broadening mechanisms and laser bandwidth. Due to possible residual Doppler broadening of about 30 MHz and a laser bandwidth of about 6 MHz (this bandwidth was not measured in our system), excited state hyperfine spacing could not be measured. Using a laser with a smaller linewidth and an optical alignment with no angle between interacting pump and probe beams, this resolution may be increased.

Further experiments with this setup could be performed to study the effects on transmitted probe polarization when the pump beam is polarized in different ways (ie to optically pump the sample). This polarization would change the relative transition strengths for the hyperfine levels in

both Lithium isotopes, thus changing the absorption depths of the resultant saturated absorption signal [15]. We also observed the saturated absorption signal change as a function of external magnetic field. Further work could explain this in terms of how the m_F states in the Lithium atoms would no longer be degenerate due to the Zeeman effect.

Chapter 6

Appendix

6.1 Laser System Control Circuits

6.1.1 Temperature Control Circuit

While the diode lasers used in our experiment output a wavelength roughly around 670 nm, further correction to the output wavelength is desired to obtain better control over the operating scanning range; Since the laser can only operate up to a certain current without breaking, it is helpful to try to modify the output wavelength in as many ways possible *before* having to "brute force" modify the output laser wavelength by modulating its supplied current. This is done by modulating the temperature of the laser itself. As the temperature of the laser is increased, redder/longer wavelengths are output. While a digital circuit can be created to accomplish this, analogue circuits tend to have a faster reaction time in supplying the correct amount of voltage to a heating resistor. Figure 6.1 shows the constructed temperature control circuit to heat the aluminum laser housing. To help determine how the temperature control circuit operates, it will be discussed piece by piece to outline how each portion of the circuit behaves.

Our voltage that is directly proportional to measured temperature of the block (V_{temp}) is controlled using an AD590 temperature sensor. This output from the AD590 is amplified through a simple inverting amplifier. The AD590 is calibrated such that there is $1\mu A/K$. The gain of the V_{temp} op amp is set such that it would produce 0 V at 20 and 10 V at 80. Follower op amps with unity gain and low pass filters were inserted prior to the BNC for each output voltage to try to produce a resultant signal with low noise.

The set voltage (set temperature for the block) is controlled using a variable resistor. The "goal" of the circuit is to try to make the set and temperature voltages the same. By taking the difference of these two voltages through a difference amplifier, the circuit is able to determine how much it needs to work in order to make this condition true. This is the upper portion of our circuit in Fig. 6.1. V_{err} is defined as the difference of

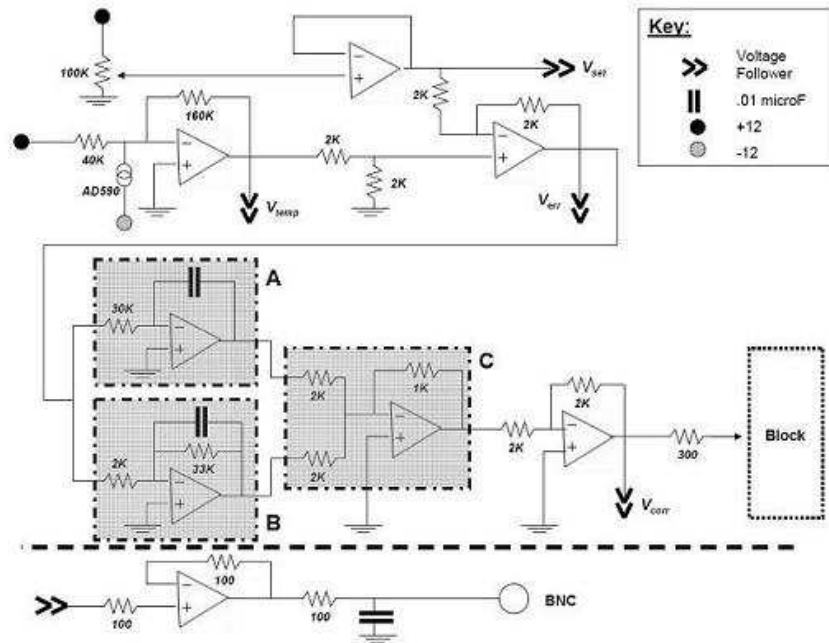


Figure 6.1: analogue temperature control circuit used to heat laser mount block

these two signals and the output of the difference amplifier. It should be noted that the circuit only functions if V_{err} is *negative*, heating up the block through current flowing through the transistors and resistor.

The circuit then goes to a “correction” portion which can be broken up into three parts:

A: This is an integrator, where

$$V_{out} = \int \frac{V_i n}{RC} dt \quad (6.1)$$

This allows the circuit to reach a steady state because if the error signal drops to zero (the two temperatures are equal) then the V_{out} is a constant. This means that the circuit is providing a steady amount of current to the heating portion to maintain the specified temperature.

B: This is an amplifier that scales the input by a gain factor. The capacitor acts as a low pass filter to reduce noise in the circuit.

C: The two inputs are summed in this summing amplifier to go to the heater block

Shown in Fig 6.2, the 5Ω resistor and transistors heat up due to their low resistance values relative to the incoming 12V.

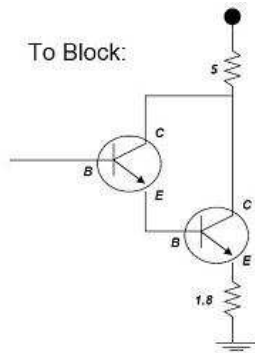


Figure 6.2: block transistor layout

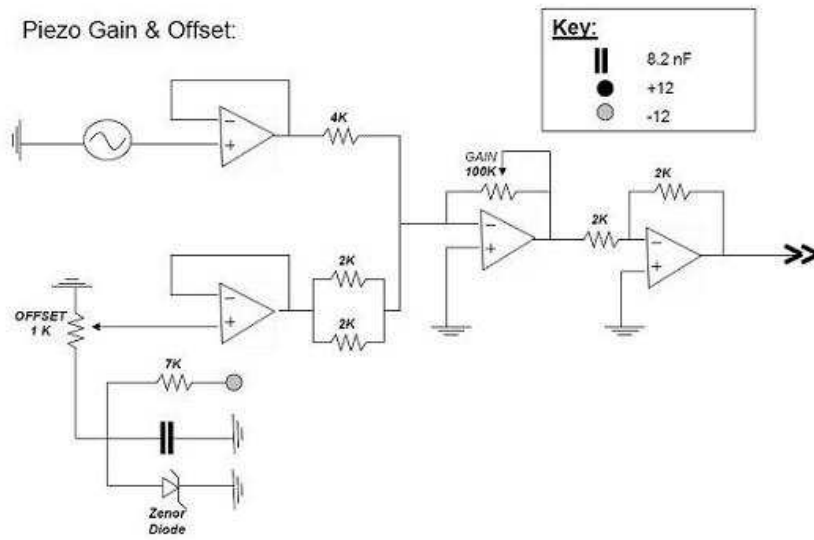


Figure 6.3: piezo controller used to modify offset and amplitude of eternal cavity oscillations

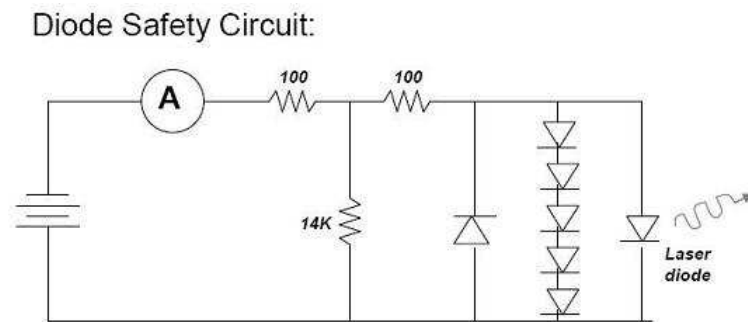


Figure 6.4: safety circuit for the laser diode to ensure the maximum current cannot exceed 50 mA

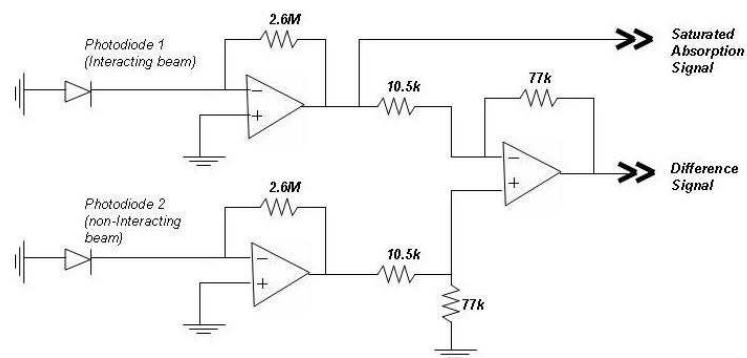


Figure 6.5: Difference amplifier for two probe beam detectors.

Bibliography

- [1] Borde, C. J. “Saturated Absorption line shape: Calculation of the transit-time broadening by a perturbation approach” *Phys. Rev. A* Vol 14 No. 1, 1976.
- [2] Bransden, B.H. & Joachain, C.J. Physics of Atoms and Molecules, 2nd Edition Essex, England: Pearson Education Limited, 2003.
- [3] Burkhardt, C & Leventhal, J. Topics in Atomic Physics New York, NY: Springer Pub., 2006.
- [4] Conroy, R.S. et al. “A visible extended cavity diode laser for the undergraduate laboratory” *Am. J. Phys.* Vol. 68 No. 10, 2000.
- [5] Demtroder, W. Laser Spectroscopy: Basic Concepts and Instrumentation. New York, NY: Springer-Verlag, 1981.
- [6] Duarte, A.E et al. “Doppler-free spectroscopy and collisional studies with tunable diode lasers of lithium isotopes in a heat-pipe oven” *J. Opt. Soc. Am. B* Vol. 15 No. 7, 1998.
- [7] Foot, C.J. Atomic Physics New York, NY: Oxford University Press, 2005.
- [8] Griffiths, David J. *Introduction to Quantum Mechanics, 2nd ed.* Prentice Hall, 2004.
- [9] Hall, J. L. “Shift and broadening of saturated absorption resonances due to curvature of laser wave fronts” *Applied Physics Letters* Vol 20 No 12, 1976.
- [10] Hilborn, R. “Einstein coefficients, cross sections, f values, dipole moments, and all that” *Am. J. Phys.* Vol. 50 No. 11, 1982.
- [11] Ikegami, T. & Inaba, H. “Atomic and Molecular spectroscopy with a continuous-wave, doubly resonant, monolithic optical parametric oscillator” *Optics Communications* Vol 269, No. 1, pg. 188-193, 2007.

- [12] Libbrecht, K.G et all. “Teaching physics with 670nm diode lasers– construction of stabilized lasers and lithium cells” *Am. J. Phys.* Vol 63 No. 8, 1995.
- [13] Melissinos, A. & Napolitano, J. Experiments in Modern Physics San Diego, CA: Academic Press, pg 243-250, 2003.
- [14] Mellish, A. & Wilson, A. “A simple laser cooling and trapping apparatus for undergraduate laboratories” *Am. J. Phys.* Vol. 70 No. 9, 2002.
- [15] Metcalf, H. & Van der Straten, P. Laser Cooling and Trapping York, PA: Springer Inc, 1999.
- [16] Ohtsuka, T. et all. “Doppler-Free Two-Photon Spectroscopy of $6S_{1/2} - 6D_{3/2,5/2}$ Transition of Cesium” *J. Phys. Jpn.* Vol. 74, No 9, 2005.
- [17] Rao, G.N. et all. “Atomic hyperfine structure studies using temperature/ current tuning of diode lasers: An undergraduate experiment” *Am. J. Phys.* Vol. 66 No. 8, 1998.
- [18] Schiller, S. “High Resolution Doppler free molecular spectroscopy with a continuous-wave optical parametric oscillator” *Optics Letters* Vol. 26 No. 18, 2001.
- [19] Terrell, M. & Masters, M. “Laser spectroscopy of the cesium dimer as a physics laboratory experiment” *Am. J. Phys.* Vol. 64, No. 9, 1996.
- [20] Tiwari, V.B et all. “Laser frequency stabilization using Doppler-free bi-polarization spectroscopy” *Optics Communications* Vol. 262, pg. 249-255, 2006.
- [21] Wieman, C. & Hansch, T.W. “Doppler-Free Laser Polarization Spectroscopy” *Phys. Review Letters* Vol. 26, No. 20, 1976.